

zircon into baddelyite and silica. Comparison of U-Xe and U-Pb ages (24) suggests that Xe is at least as strongly retained as Pb. Nevertheless, Pb loss associated with metamictization is commonly observed in zircons (25), and, given the antiquity and complex history of the ancient detrital zircons, it is likely that loss of Xe will also have occurred in a portion of our samples.

We have developed a two-stage model to show how the $^{131}\text{Xe}/^{136}\text{Xe}$ ratios are affected by Xe loss during diffusion or recrystallization events and provide an illustration for zircons with a crystallization age of 4.2 Gy and initial Pu/U = 0.006 (Fig. 3). Early events cause the loss of predominantly Pu-fission xenon, and the subsequent buildup is dominated by xenon from U. In consequence, the present-day $^{131}\text{Xe}/^{136}\text{Xe}$ ratio is lowered, reaching a minimum for loss occurring around 3.5 to 3.8 Ga. As the time of Xe loss approaches the present, the short time available for U fission ingrowth relative to the amount of Pu xenon results in measured $^{131}\text{Xe}/^{136}\text{Xe}$ ratios that approach the value they would have if no loss had occurred. The $^{131}\text{Xe}/^{136}\text{Xe}$ ratio is thus most sensitive to Xe loss during Archean events. This suggests that the low $^{131}\text{Xe}/^{136}\text{Xe}$ ratios in the discordant Jack Hills zircons may be the result of events before the formation of the Jack Hills metasediments. To be more definitive requires an additional relationship between the time of Xe loss and the degree of loss. Such a relationship can in principle be provided by the simultaneous determination of U-Xe ages.

We have detected Xe with an isotopic composition characteristic of the spontaneous fission of ^{244}Pu in individual 4.1- to 4.2-Gy-old detrital zircons. The initial Pu/U ratios, at 4.56 Ga, implied by our analyses range from essentially zero to 0.0066 between individual zircons. This is probably the result of Xe loss during subsequent metamorphic processes, e.g., those associated with formation of the host metasediments. Combining the present procedures with U-Xe dating methods has the potential to date these early metamorphic processes. The highest implied Pu/U ratio is within the range of estimates from meteorites, but, in order to quantify a global Pu/U ratio for the early Earth, future work will require an improved understanding of the geochemical behavior of Pu relative to U and the rare earth elements in zircon crystallization.

References and Notes

- B. S. Meyer, D. D. Clayton, *Space Sci. Rev.* **92**, 332 (2000).
- D. D. Clayton, *Astrophys. J.* **268**, 381 (1983).
- G. J. Wasserburg, M. Busso, R. Gallino, *Astrophys. J.* **466**, L109 (1996).
- S. Goriely, M. Arnould, *Astron. Astrophys.* **379**, 1133 (2001).
- A. G. W. Cameron, F.-K. Thielemann, J. J. Cowan, *Phys. Rep.* **227**, 283 (1993).
- T. Staudacher, C. J. Allegre, *Earth Planet. Sci. Lett.* **60**, 389 (1986).
- C. J. Allegre et al., *Nature* **303**, 762 (1983).
- C. J. Allegre et al., *Earth Planet. Sci. Lett.* **81**, 127 (1986).
- R. K. O'Nions, I. N. Tolstikhin, *Earth Planet. Sci. Lett.* **124**, 131 (1994).
- D. Porcelli, G. J. Wasserburg, *Geochim. Cosmochim. Acta* **59**, 4921 (1995).
- J. Kunz, T. Staudacher, C. J. Allegre, *Science* **280**, 877 (1998).
- G. B. Hudson, B. M. Kennedy, F. P. Podosek, C. M. Hohenberg, *Proc. Lunar Planet. Sci. Conf.* **19**, 547 (1989).
- G. W. Lugmair, K. Marti, *Earth Planet. Sci. Lett.* **35**, 273 (1977).
- F. Shukolyukov, F. Begemann, *Geochim. Cosmochim. Acta* **60**, 2453 (1996).
- Y. N. Miura, K. Nagao, N. Sugiura, T. Fujitani, P. H. Warren, *Geochim. Cosmochim. Acta* **62**, 2369 (1998).
- P. Pellas, C. Fieni, M. Trierloff, E. K. Jessberger, *Geochim. Cosmochim. Acta* **61**, 3477 (1997).
- M. Honda, A. P. Nutman, V. C. Bennett, *Earth Planet. Sci. Lett.* **207**, 69 (2003).
- D. O. Froude et al., *Nature* **304**, 616 (1983).
- S. A. Wilde, J. W. Valley, W. H. Peck, C. M. Graham, *Nature* **409**, 175 (2001).
- S. J. Mojzsis, T. M. Harrison, R. T. Pidgeon, *Nature* **409**, 178 (2001).
- T. M. Harrison, S. J. Mojzsis, *Geochim. Cosmochim. Acta* **67**, A135 (2003).
- J. D. Gilmour, I. C. Lyon, W. A. Johnston, G. Turner, *Rev. Sci. Instr.* **65**, 617 (1994).
- Materials and methods are available as supporting material on Science Online.
- Yu. A. Shukolyukov, A. P. Meshik, D. P. Krylov, O. V. Pravdivtseva, in *Noble Gas Geochemistry and Cosmochemistry*, J. Matsuda, Ed. (Terra Science, Tokyo, 1994), p. 125.
- T. E. Krogh, *Geochim. Cosmochim. Acta* **46**, 637 (1982).
- This work was supported by grants from Particle Physics and Astronomy Research Council (G.H.), the Australian Research Council, NSF Division of Earth Sciences Infrastructure and Facilities program (T.M.H.) and NASA Exobiology Program (S.J.M.). Technical help from A. Busfield and R. Mohapatra in the RELAX laboratory is gratefully appreciated.

Supporting Online Material

www.sciencemag.org/cgi/content/full/306/5693/89/DC1

Materials and Methods

Figs. S1 to S4

2 June 2004; accepted 13 August 2004

Geochemical Evidence for Excess Iron in the Mantle Beneath Hawaii

Munir Humayun,^{1,2*} Liping Qin,¹ Marc D. Norman³

Chemical interaction of Earth's mantle with the liquid outer core should influence the mantle's iron content. Osmium isotope ratios in Hawaiian lavas indicate a mass flux of $\leq 1\%$ core to the mantle, which is the immediate source of these lavas. We present precise measurements of the Fe/Mn ratio for Hawaiian lavas, revealing an increase of 1 to 2% in the mole fraction of iron in the mantle beneath Hawaii. This corresponds to a density anomaly of about 0.5%, about the same magnitude observed in seismic tomography models of the Pacific superswell region. These data also rule out a role for Mn-rich sediments as the source of the Hawaiian Os isotope signal.

On the basis of geophysical evidence, some mantle plumes are argued to arise from the core-mantle boundary (CMB). Chemical interaction between the core and the mantle at the CMB may involve physical entrainment of differentiated outer core (1), disequilibrium chemical reactions (2), equilibrium chemical reactions (3, 4), isotopic exchange (5), or exsolution of a light element component during inner core growth (4, 6), each of which may impart distinct isotopic and chemical signatures to the adjacent mantle. Assuming that the effects of chemical interaction are localized to mantle adjacent to the CMB, plumes arising from the CMB may entrain mantle that has experienced core-mantle interaction and advect such chemical signatures to the sur-

face where they may be detected in the chemistry of erupted lavas. Osmium isotopic composition of Hawaiian picrites has provided the best indication for the entrainment of differentiated outer core material in the source of the Hawaiian plume, implying a mass flux $\leq 1\%$ by weight (1). The absence of unradiogenic $^{182}\text{W}/^{184}\text{W}$ in the Hawaiian picrites, however, has been taken as evidence against core-mantle interaction (7). It has also been used to support the suggestion that the observed Re-Pt-Os isotope systematics (1) can be explained by the recycling of surficial Mn sediments (with high Pt/Os and Pt/Re ratios) into the source of the Hawaiian plume (7, 8). Evidence of Mn enrichment was not found in Gorgona Island komatiites, which exhibited coupled ^{186}Os - ^{187}Os isotope variations (9).

Iron, the dominant constituent of the core, is probably the most important element with a geochemical cycle that can be affected by exchange across the CMB. The Fe flux is of primary concern in geodynamic models, because it influences the density of the mantle (10–12). The constant molar 100 Mg/Mg+Fe (Mg#) is 89 ± 2 (1 σ) of

¹Department of the Geophysical Sciences, 5734 South Ellis Avenue, Chicago, IL 60637, USA. ²National High Magnetic Field Laboratory and Department of Geological Sciences, Florida State University, Tallahassee, FL 32310, USA. ³Research School of Earth Sciences, Australian National University, Canberra ACT 0200, Australia.

*To whom correspondence should be addressed. E-mail: humayun@magnet.fsu.edu

primitive mantle xenoliths, which implies that the upper mantle contains $6.26 \pm 0.63\%$ (1σ) Fe as FeO dissolved in minerals (13). From seismic tomography and mineral physics constraints, the lower mantle is inferred to possibly contain 10 to 20% higher Fe (10–12). The inferred excess Fe may be primordial (4), the result of recycling of Fe-rich crust (10), or the result of Fe exchange across the CMB (11). Notably, the present uncertainties (10%, 1σ) assigned to upper mantle Fe abundances are comparable to the expected excess Fe in lower mantle derived plumes. Geochemical evidence for excess Fe in mantle-derived melts has been further limited by chemical fractionation of Fe from Mg and other elements during partial melting and fractionation (14). Here, we present a refined method that uses Fe/Mn ratios to determine excess Fe abundances in the sources of mantle-derived magmas.

Because most of the Fe in the mantle is Fe^{+2} (FeO) and all of the Mn is Mn^{+2} (MnO), Fe and Mn share the same charge and have a similar ionic radius, the two properties that most influence the partitioning behavior of elements in magmatic processes. During partial melting and fractional crystallization, the abundance of Mn^{+2} follows that of Fe^{+2} , so the Fe/Mn ratio should remain approximately constant. The coherence of the Fe and Mn geochemical cycles in the mantle is not followed by sedimentary processes or by core-mantle interaction, because Fe or Mn occurs in other valence states. A global suite of mantle peridotites yields $Fe/Mn = 60 \pm 10$ (1σ) (13), whereas a similar comparison of basalts yields $Fe/Mn = 59 \pm 9$ (1σ) (15). The scatter of existing measurements of the Fe/Mn ratio in basalts from a single tectonic setting conceals the variations predicted by geophysical models. Because a substantial part of this scatter may be due to analytical artifacts (15), a new technique based on inductively coupled plasma mass spectrometry (ICP-MS) has been developed for the precise ($\pm 0.5\%$) determination of the Fe/Mn ratio of fresh basalts (16).

Our measurements resolve Hawaiian picrites from mid-ocean ridge basalts (MORBs) or Icelandic picrites (Fig. 1A). Unlike radiogenic isotope ratios, the Fe/Mn ratio may be affected by the degree of partial melting, the residual mantle mineralogy, and the extent of olivine fractionation or accumulation experienced by the lavas. Given that olivine has a higher Fe/Mn ratio, olivine removal from the melt should decrease the Fe/Mn ratio of erupted lava, whereas olivine accumulation should increase the Fe/Mn ratio. One test of the precision of the data is to observe Fe/Mn variations associated with olivine fractionation (Fig. 1B; data are plotted individually for each volcano). Using estimates of the

MgO content of primary magma (magma composition before crystal fractionation or accumulation) (17), we determined the primary magma Fe/Mn ratio (Table 1). The excess Fe/Mn in Hawaiian picrites relative to MORB is not the result of olivine accumulation, given that Icelandic picrites with the same MgO range as Hawaiian picrites show Fe/Mn similar to MORBs, and three Kilauea basalts also exhibit an $Fe/Mn > 65$. Fur-

thermore, Fig. 1 shows that the high Fe/Mn ratio is characteristic of picrites and basalts from Loihi, Kilauea, Mauna Kea, Mauna Loa, Hualalai, Kohala, and Koolau (i.e., the entire Hawaiian plume).

Explanations of the radiogenic $^{186}Os/^{188}Os$ ratios in terms of recycling of Mn-rich sediments (7, 8) imply that $Fe/Mn \leq 40$, substantially lower than the mantle value of 60. Mixing models involving Mn-sediment

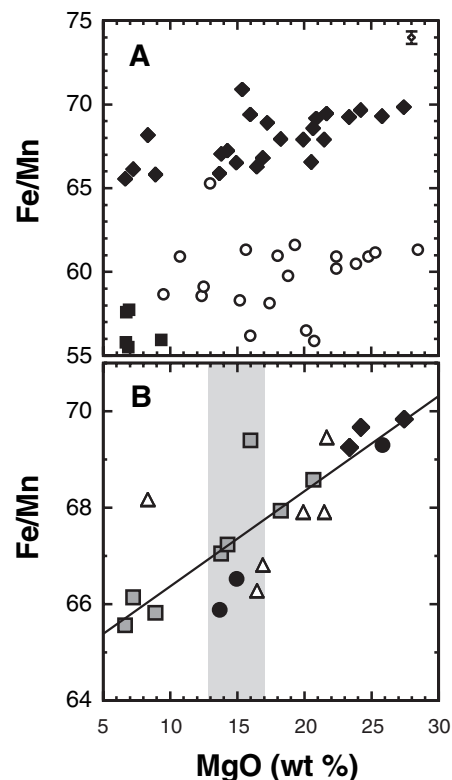


Fig. 1. (A) Fe/Mn determined by ICP-MS versus MgO for Hawaiian lavas (diamonds), Icelandic picrites (circles), and MORB glasses (squares). A representative error bar (2σ) (open diamond) is shown in the upper right-hand corner. (B) An expansion of the scale for the Hawaiian lavas, showing suites for which three or more samples from the same volcano were analyzed: Kilauea (squares), Loihi (diamonds), Mauna Loa (triangles), and Hualalai (circles). Each suite forms an olivine fractionation or accumulation trend; Kil 1-7 and MLKAH-4 deviate from the trends for no apparent reason. The shaded field depicts the range of estimated primitive melt MgO contents for the Hawaiian picrites (17).

Table 1. Fe/Mn (weight ratio) corrected for olivine gain/loss, mole fraction of Fe, Mg#, and density anomaly, inferred in the source of Hawaiian volcanoes (16). δX_{Fe} , the anomaly in the mole fraction of Fe; PUM, primitive upper mantle.

	Fe/Mn	X_{Fe}	δX_{Fe}	Mg#	$\delta\rho/\rho$ (%)
Kilauea	67.4 ± 0.4	0.1189 ± 6	0.017	88.11 ± 0.06	$+0.55 \pm 0.06$
Mauna Loa	65.8 ± 0.9	0.1164 ± 14	0.015	88.36 ± 0.14	$+0.47 \pm 0.07$
Hualalai	66.4 ± 0.5	0.1173 ± 8	0.016	88.27 ± 0.08	$+0.50 \pm 0.06$
Iceland	59.5 ± 1.5	0.1064 ± 24	0.005	89.36 ± 0.24	$+0.15 \pm 0.10$
MORB	56.5 ± 1.1	0.1016 ± 18	≈ 0	89.84 ± 0.18	≈ 0
PUM (13)	60 ± 10	0.107 ± 16	0.006	89.3 ± 1.6	$+0.18 \pm 0.51$

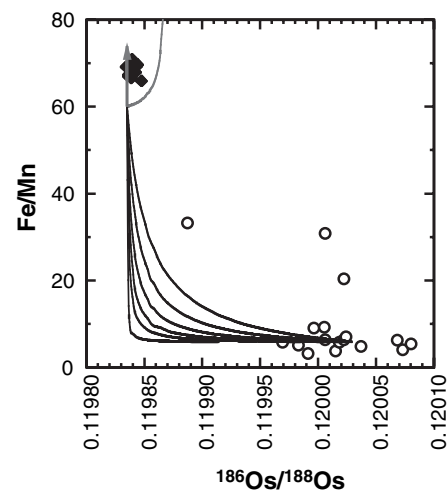


Fig. 2. Fe/Mn versus $^{186}Os/^{188}Os$ (7) for the Hawaiian picrites (black diamonds) compared with model predictions for mixing between recycled Mn-rich sediment (black curves), outer core (gray curves), and normal mantle. The Pt/Os ratios of the Troodos umbers (7) were used to calculate the $^{186}Os/^{188}Os$ ratios for these sedimentary compositions after 2 Ga of radiogenic ingrowth (circles). Mixing lines were calculated between average sediment [6.5% Mn, $Fe/Mn = 5.8$, $Os = 230$ parts per trillion (ppt) (7), $^{186}Os/^{188}Os = 0.12003$], and peridotite [Mn = 0.1045%, $Fe/Mn = 60$ (13); $Os = 3800$ ppt, $^{186}Os/^{188}Os = 0.1198345$ (1)] or picrite [Mn = 0.13%, $Fe/Mn = 60$, $^{186}Os/^{188}Os = 0.1198345$ (1, 17)] and are hyperbolic concave downward. The most hyperbolic curve is that for normal mantle, with successive picrite curves for 800, 400, 200, 100, and 50 ppt Os, respectively. Mixtures between mantle and outer core [parameters from (9, 13)] are shown as gray curves. The $Fe/Mn > 65$ for Hawaiian picrites are compatible with a combination of FeO metasomatism (gray vertical arrow) and outer core admixture (gray hyperbola).

recycling/assimilation by peridotite, picrites, or basalts fail to increase the $^{186}\text{Os}/^{188}\text{Os}$ ratio without lowering the value of Fe/Mn (Fig. 2).

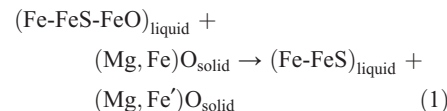
Three hypotheses may explain the elevated Fe/Mn value of Hawaiian lavas relative to MORB or Icelandic picrites: (i) partial melting of low-olivine mantle, (ii) pyroxenite melt contributions, and (iii) Fe flux across the CMB. To assess the effect of mineralogical control on the Fe/Mn ratio of mantle melts, Fig. 3A shows the partition coefficients (D) for Fe and Mn in major phases for experimental melts of garnet peridotite (18). Both D(Fe) and D(Mn) are <1 in all phases (i.e., both elements are mildly incompatible). Olivine exhibits $D(\text{Fe}) > D(\text{Mn})$, garnet and clinopyroxene exhibit the reverse effect, and orthopyroxene is intermediate in its Fe/Mn preference. Thus, melts derived from spinel and garnet peridotites exhibit an Fe/Mn value slightly lower than that of their source region (between 55 and 58 versus 61) (Fig. 3, B and C). The presence of olivine in the residual mantle counterbalances the effect of garnet and clinopyroxene on the Fe/Mn ratio of the melt such that no systematic large deviations of the Fe/Mn ratio for mantle-derived melts occur (Fig. 3A). The proportions of garnet and clinopyroxene are important in controlling the abundances of the rare earth elements and are well estimated in the Hawaiian source (17). But the ratio of olivine to orthopyroxene is not similarly constrained, so if the Hawaiian source were substantially more Si-rich (<25% olivine in the source), then the resulting partial melts could exhibit higher

Fe/Mn ratios. However, no other evidence supports a Si-rich mantle, with the exception of Koolau (17).

Recycling of MORB crust (Fe/Mn ~ 55 to 58) should not increase the Fe/Mn value of the source, but could increase the Fe/Mn ratio of partial melts derived from pyroxenite veins due to mineralogical control by clinopyroxene and garnet. Experimental studies of the partial melting of MORB-composition pyroxenites (19, 20) show that the Fe/Mn value of pyroxenite melts decreases as the degree of partial melting increases; melts formed by over 60% partial melting (MgO > 5%) show no deviation from their source composition (Fig. 3C). However, because peridotite melting only begins at temperatures at which such pyroxenites are over 60% melted (19), pyroxenite partial melts cannot contribute substantially to the high Fe/Mn ratio of the Hawaiian picrites. Silica-undersaturated pyroxenite melts (21) provide a more potent end-member. The addition of 25% of melt V162 (21) to basalt with Fe/Mn ~ 58 produces a liquid with Fe/Mn ~ 66. However, the amount of pyroxenite contribution to the sources of the various Hawaiian picrites was estimated from trace element abundances to be negligible for all but the Koolau lavas, in which it is <10% (17). No systematic difference of Fe/Mn between Koolau and other lavas can be discerned (fig. S2), indicating that the effect of pyroxenite melting on the Fe/Mn ratio is minor. It must be concluded that the high Fe/Mn value is a feature of the source composition and not of the melting process.

Oxygen (as FeO) is a likely candidate for the light element in the core (22). The exchange of FeO between the core and the lower mantle may occur during core formation processes as FeO-saturated melts percolate through the lower mantle (4), or FeO may exsolve from the outer core as the inner core grows (5, 23), creating the seismic anomalies observed at the CMB (11, 24). For the outer core, Fe/Mn > 170 (13). Thus, FeO exchange between the liquid outer core occurring either in the ancient Earth, or actively over time, would impart a high Fe/Mn to regions of the lower mantle. The Hawaiian plume may have entrained small amounts of a FeO-rich layer from the CMB (25) or entrained lower mantle with primordially high FeO contents (4, 10). This raises an important question: Why is the Fe/Mn ratio not correlated with radiogenic $^{186}\text{Os}/^{188}\text{Os}$ ratios observed in the picrites?

Both modern liquid outer core and ancient percolating melts may be composed of an FeO-FeS-Fe liquid (22), which would react with the lower mantle mineralogy (Mg perovskite and ferropericlae). Reactions between a FeO-FeS-Fe liquid and ferropericlae can be written in a simplified form as



where the prime indicates a solid solution richer in FeO. Because oxygen is only

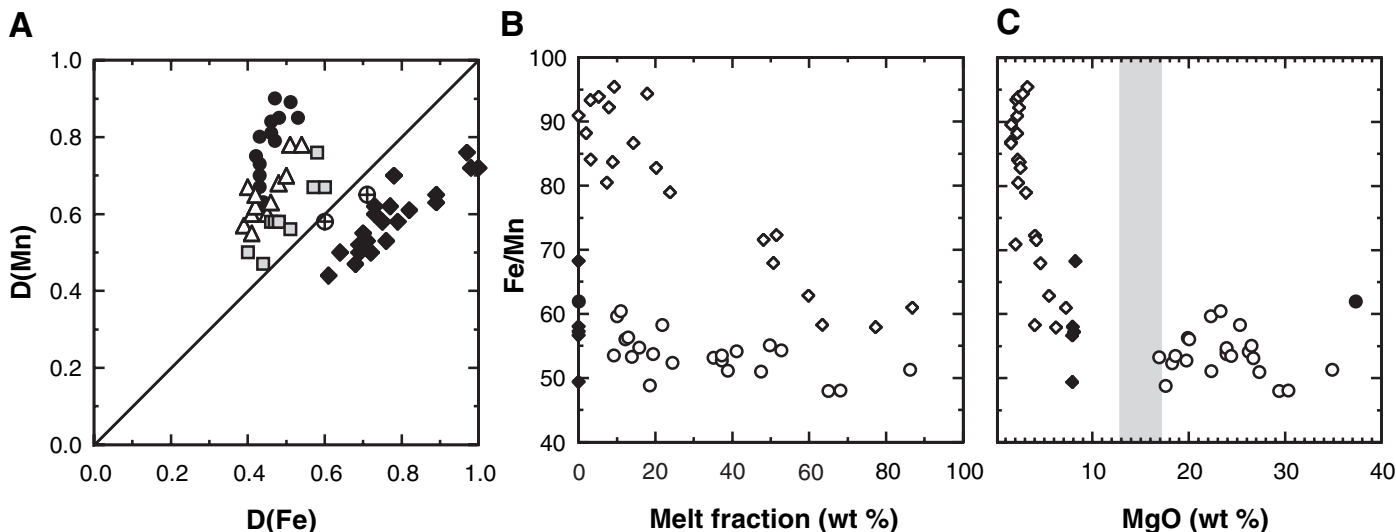


Fig. 3. (A) Partition coefficients for Fe versus Mn in olivine (diamonds), orthopyroxene (squares), clinopyroxene (triangles), and garnet (circles) from experimental melting of garnet peridotite (18). Bulk partitioning for peridotite compositions with 55% olivine, 25% orthopyroxene, 10% clinopyroxene, and 10% garnet is shown for two runs in which all four minerals and liquids were present (circled crosses). Note the Mn preference of garnet and clinopyroxene, the Fe preference of olivine, and the tendency of the bulk Ds to plot near the 1:1 line. (B) Fe/Mn of

experimental partial melts versus melt fraction: garnet peridotite melts (open circles) and their starting composition (solid circle) (18), pyroxenite melts (open diamonds) and their starting compositions (solid diamonds) (20). (C) Fe/Mn for experimental partial melts versus MgO for garnet peridotite (18) and pyroxenite (20) [symbols as in (B)]. The shaded gray region is the MgO range estimated for primitive Hawaiian picrite melts (17). High-degree (>60%) pyroxenite partial melts and all peridotite partial melts exhibit Fe/Mn < 60.

slightly soluble in iron metal at the pressure of the CMB (23), Reaction 1 represents a net transfer of FeO to ferroprecipitate. The residual Fe-FeS liquid is probably immiscible with the lower mantle and either drains back to the core or crystallizes within the lower mantle as Fe-FeS veins. Thus, large regions of the lower mantle may be metasomatized by FeO-bearing liquids creating high Fe/Mn sources, with siderophile Os [and hence the outer core $^{186}\text{Os}/^{188}\text{Os}$ signature (1)] heterogeneously distributed within the source as veins. Because tungsten has a lower preference for solid metal than does Os (26), W and Os could be decoupled by fractional crystallization of the Fe-FeS melts. Thus, coupling between $^{182}\text{W}/^{184}\text{W}$, $^{186}\text{Os}/^{188}\text{Os}$, and Fe/Mn is not a prerequisite for evidence of core-mantle interaction.

Seismic studies indicate a correlation between ultralow-velocity zones (ULVZs) at the CMB, interpreted to be regions of partial melt, and the distribution of hot spots at the surface (27). There also appear to be rigid zones at the top of the core that correspond with ULVZs in the CMB region (28) that may be sites of FeO release from the core (5). Thus, the sources of mantle plumes originating from the CMB may have been affected by FeO metasomatism. This is the most tenable explanation at present for the observed excess of Fe/Mn in the Hawaiian lavas. Notably, Iceland neither is associated with a ULVZ (29) nor exhibits high Fe/Mn.

Table 1 shows that the observed Fe/Mn ratio in the Hawaiian lavas corresponds to a lower Mg# (88) than average upper mantle (Mg# = 89). This Mg# is within the 1σ range of measured Mg#'s of upper mantle peridotites [89 ± 2 (13)]. The higher FeO content implies a higher density, +0.5% relative to MORB mantle. This density contrast is about twice that estimated from seismic tomography models (12) but is sensitive to the choice of MORB Fe/Mn for normalization (Table 1). It is important to observe that our estimate of the density anomaly $\delta\rho/\rho$ does not include the effect of Fe enrichment due to recycling crust with a Fe/Mn ~ 60 because this contribution is not resolved by our technique. However, core-mantle interaction appears to have added enough FeO to the Hawaiian plume source to account for some (10) or all (11, 12) of the geophysically observed density excess in the lower mantle. Thus, Fe/Mn analysis of hot spot lavas provides geochemical "ground truth" to geodynamical models of mantle circulation based on seismic tomography (12, 29).

References and Notes

1. A. D. Brandon, M. D. Norman, R. J. Walker, J. W. Morgan, *Earth Planet. Sci. Lett.* **174**, 25 (1999).
 2. E. Knittle, R. Jeanloz, *Science* **251**, 1438 (1991).
 3. D. Walker, *Geochim. Cosmochim. Acta* **64**, 2897 (2000).

4. D. C. Rubie, C. K. Gessmann, D. J. Frost, *Nature* **429**, 58 (2004).
 5. I. S. Puchtel, M. Humayun, *Geochim. Cosmochim. Acta* **64**, 4227 (2000).
 6. B. Buffett, E. J. Garnero, R. Jeanloz, *Science* **290**, 1338 (2000).
 7. A. Schersten, T. Elliott, C. Hawkesworth, M. Norman, *Nature* **427**, 234 (2004).
 8. G. Ravizza, J. Blusztajn, H. M. Prichard, *Earth Planet. Sci. Lett.* **188**, 369 (2001).
 9. A. D. Brandon *et al.*, *Earth Planet. Sci. Lett.* **206**, 411 (2003).
 10. L. H. Kellogg, B. H. Hager, R. D. van der Hilst, *Science* **283**, 1881 (1999).
 11. E. J. Garnero, *Annu. Rev. Earth Planet. Sci.* **28**, 509 (2000).
 12. A. M. Forte, J. X. Mitrovica, *Nature* **410**, 1049 (2001).
 13. W. F. McDonough, S.-s. Sun, *Chem. Geol.* **120**, 223 (1995).
 14. C. H. Langmuir, G. N. Hanson, *Philos. Trans. R. Soc. London Ser. A* **297**, 383 (1980).
 15. A. Ruzicka, G. A. Snyder, L. A. Taylor, *Geochim. Cosmochim. Acta* **65**, 979 (2001).
 16. Materials and methods are available as supporting material on Science Online.
 17. M. D. Norman, M. O. Garcia, *Earth Planet. Sci. Lett.* **168**, 27 (1999).
 18. M. J. Walter, *J. Petrol.* **39**, 29 (1998).
 19. M. Pertermann, M. M. Hirschmann, *J. Geophys. Res.* **108**, 2125, 10.1029/2000JB000118 (2003).
 20. M. Pertermann, M. M. Hirschmann, *J. Petrol.* **44**, 2173 (2003).
 21. T. Kogiso, M. M. Hirschmann, D. J. Frost, *Earth Planet. Sci. Lett.* **216**, 603 (2003).
 22. J.-P. Poirier, *Phys. Earth Planet. Inter.* **85**, 319 (1994).
 23. Experimental results of Rubie *et al.* (4) were extrapolated to 128 to 136 GPa and 2600 to

3000K with the use of their equation 2 to obtain the molar metal-silicate partition coefficient, $K_d \leq 6 \times 10^{-4}$. Setting $X_{\text{Fe}}^{\text{metal}} \sim 1$, $X_{\text{Fe}}^{\text{Mg-wüstite}} \sim 0.2$, where X represents the mole fraction, in their definition of K_d yields $X_{\text{O}}^{\text{metal}} \leq 1 \times 10^{-4}$. These experiments imply that metallic liquids in equilibrium with lower mantle mineralogy should be very low in oxygen content and that FeO should be released from the core to the mantle at the CMB, if oxygen is present in the outer core at 9 weight percent (wt %) (FeO = 40 wt %) (22).
 24. T. Lay, Q. Williams, E. J. Garnero, *Nature* **392**, 461 (1998).
 25. A. M. Jellinek, M. Manga, *Nature* **418**, 760 (2002).
 26. N. L. Chabot, A. J. Campbell, J. H. Jones, M. Humayun, C. B. Agee, *Meteoritics Planet. Sci.* **38**, 181 (2003).
 27. Q. Williams, J. Revenaugh, E. Garnero, *Science* **281**, 546 (1998).
 28. S. Rost, J. Revenaugh, *Science* **294**, 1911 (2001).
 29. A. M. Jellinek, M. Manga, *Rev. Geophysics* **42**, RG3002, 10.1029/2003RG000144 (2004).
 30. We thank S. Sorenson (Smithsonian Institution) and A. T. Anderson for providing samples; A. J. Campbell for support on the Element; and A. D. Brandon, B. Buffett, M. Hirschmann, and C. Langmuir for comments and discussions. Constructive reviews by C.-T. Lee and P. Reiners are gratefully acknowledged. NSF EAR-0309786 (M.H.) supported this work.

Supporting Online Material

www.sciencemag.org/cgi/content/full/306/5693/91/DC1

Materials and Methods

Figs. S1 and S2

Tables S1 and S2

References

3 June 2004; accepted 17 August 2004

Toroidal Triblock Copolymer Assemblies

Darrin J. Pochan,^{1*} Zhiyun Chen,^{2†} Honggang Cui,^{1†} Kelly Hales,^{1†} Kai Qi,^{2†} Karen L. Wooley^{2*}

A stable phase of toroidal, or ringlike, supramolecular assemblies was formed by combining dilute solution characteristics critical for both bundling of like-charged biopolymers and block copolymer micelle formation. The key to toroid versus classic cylinder micelle formation is the interaction of the negatively charged hydrophilic block of an amphiphilic triblock copolymer with a positively charged divalent organic counterion. This produces a self-attraction of cylindrical micelles that leads to toroid formation, a mechanism akin to the toroidal bundling of semiflexible charged biopolymers such as DNA. The toroids can be kinetically trapped or chemically cross-linked. Insight into the mechanism of toroid formation can be gained by observation of intermediate structures kinetically trapped during film casting.

Simple self-assembly methods can produce a broad range of intricate bioinspired nanostructures from synthetic block copolymers in dilute solution. For example, robust vesicles have been constructed from amphiphilic diblock copolymers (1–3). By using block copolymers instead of low-molecular weight

lipid amphiphiles, direct control over the membrane thickness is achieved and the ultimate toughness of the vesicle is consequently enhanced (1, 4). Similarly, cylindrical micelles exhibit stiffness behavior that is directly dependent on the core chemistry (5) or chain length (6). Such cylindrical structures have been designed to display specific coronal chemistry for biomimetic inorganic phase nucleation (7, 8). Many examples of spherical micellar assemblies also exist in which the particle size and function can be controlled by means of block copolymer segment designs (9). In addition to the classic geometries of sphere, cylinder, and bilayer membrane, dilute block copolymers

¹Materials Science and Engineering and Delaware Biotechnology Institute, University of Delaware, Newark, DE 19716, USA. ²Center for Materials Innovation and Department of Chemistry, Washington University in Saint Louis, One Brookings Drive, CB 1134, Saint Louis, MO 63130, USA.

*To whom correspondence should be addressed.

†These authors contributed equally to this work.